Development of intravenously administered synthetic RNA virus immunotherapy for the treatment of cancer

Edward Kennedy
Oncorus, Inc.
Agnieszka Denslow
Oncorus, Inc.
Jacqueline Hewett
Oncorus, Inc.
Lingxin Kong
Oncorus, Inc.
Ana De Almeida
Oncorus, Inc.
Jeffrey Bryant
Oncorus, Inc.
Jennifer Lee
Oncorus, Inc.
Judy Jacques
Oncorus, Inc.
Sonia Feau
Oncorus, Inc.
Melissa Hayes
Oncorus, Inc.
Elizabeth McMichael
Oncorus, Inc.
Amal Rahmeh
Pompeu Fabra University
Lauren Herschelman
Oncorus, Inc.
Danielle Douglas
Oncorus, Inc.
Jacob Spinale
Oncorus, Inc.
Sanmit Adhikari

Oncorus, Inc.
Jessica Deterling
Oncorus, Inc.
Matt Scott
Oncorus, Inc.
Brian Haines
Oncorus, Inc.
Mitchel Finer
ElevateBio, Inc.,
Ted Ashburn
Oncorus, Inc.
Christophe Quéva
Oncorus, Inc.
Lorena Lerner (lorena.lerner@Oncorus.com)
Oncorus, Inc.

Article

Keywords: oncolytic virus, immunotherapy, nanoparticle, RNA therapeutics, intravenous, cancer, synthetic RNA virus

Posted Date: May 27th, 2021

DOI: https://doi.org/10.21203/rs.3.rs-523458/v1

Version of Record: A version of this preprint was published at Nature Communications on October 7th, 2022. See the published version at https://doi.org/10.1038/s41467-022-33599-w.

Abstract

Oncolytic viruses (OVs) are an emerging therapeutic approach for the treatment of cancer. Clinical benefit has been demonstrated for intratumoral administration, but the therapeutic effectiveness of intravenous delivery has been limited by neutralizing antibody responses against the virus. To circumvent this limitation, we developed Synthetic RNA viruses, a novel approach for intravenous and repeated administration of OVs, consisting of a viral RNA genome (vRNA) formulated within lipid nanoparticles. For two Synthetic RNA virus drug candidates, Seneca Valley virus (SVV) and Coxsackievirus A21 (CVA21), we demonstrate vRNA delivery, viral replication, spread, and lysis of tumor cells leading to potent anti-tumor efficacy, even in the presence of OV neutralizing antibodies in the bloodstream. Synthetic-SVV replication in tumors promoted immune cell infiltration and enhanced anti-tumor activity in combination with anti-PD-1 checkpoint inhibitor. Altogether, the Synthetic RNA virus platform provides an innovative approach that enables repeat intravenous administration of viral immunotherapy.

Introduction

Oncolytic viruses (OVs) are an attractive cancer therapeutic modality that selectively kills tumor cells and inflame the tumor microenvironment (TME). Combining OVs with cancer immunotherapies has the potential to overcome immune suppression in the TME and improve their therapeutic benefit in poorly- or non-responsive tumors. Thus far, the therapeutic benefit of oncolytic virotherapy has been limited to intratumoral administration and requires a systemic antitumor immune response to be effective against non-injected lesions. Talimogene laherparevec (Imlygic®)[1], the only approved OV in the US, has demonstrated improved responses in melanoma patients only when administered intratumorally. Intravenous (IV) delivery of OVs would enhance efficacy by exposing all tumor sites, including small metastatic lesions, to the oncolytic agent. However, IV administration of OVs remains a challenge since the rapid development of neutralizing antibodies against the virus limits its exposure to tumor cells[2,3].

To maximize viral immunotherapy's potential, repeat intravenous delivery must be addressed. Retargeting[4,5], cell carriers[6,7], coating with polymers[8-10], and liposomes[11,12] have been utilized to avoid the neutralization of OV in circulation but, to date, none have progressed to the clinic. Advances in nanotechnology and delivery of nucleic acid are paving the way for new carrier systems to overcome OVs IV administration challenges[13,14].

Here, we have developed a new nanoparticle-based delivery platform that enables repeat IV administration of viral immunotherapies. Plasmid templates were engineered and optimized for *in vitro* transcription (IVT) of viral genomes, yielding viral RNA genomes (vRNA) that, upon formulation in lipid nanoparticles (LNP), rendered particles with the desired biophysical properties to support repeat IV administration. All components are synthetic, and this modality is referred to as Synthetic RNA virus.

For this study, we selected two picornaviruses OVs, Seneca Valley virus (SVV) and Coxsackievirus A21 (CVA21), based on their oncolytic activity and well-documented clinical safety[15-18]. Their genomes are

positive-sense, single-stranded RNA (~7.4 kb); they do not integrate into host chromosomes and are sufficient to initiate the entire viral lifecycle after introduction into a permissive tumor cell, making picornaviruses ideal for the Synthetic vRNA immunotherapy platform.

This study assessed the vRNA delivery and replication of Synthetic-SVV and -CVA21, confirmed oncolysis and viral spread in tumor cells and evaluated anti-tumor efficacy in multiple tumor models. We anticipate these findings will address the limitations frequently associated with IV repeated administration of OVs and further enhance the benefit of OVs in cancer therapy.

Results

Viral RNA encapsulated in LNP recapitulates OV therapy when administered intravenously. To bypass neutralizing antibodies generated that curtail the activity of IV-administered OVs, we developed Synthetic RNA viruses for systemic delivery of vRNA genomes to tumor cells. Once the vRNA/LNP is internalized and released from the endosome inside the cytoplasm of a tumor cell, the vRNA replicates and generates a burst of infectious virions that spread locally, killing adjacent tumor cells and promoting the recruitment of immune cells to the TME (Fig. 1). Picornaviruses SVV and CVA21 vRNA constructs were validated *in vitro* and *in vivo* (Supplementary Fig. 1 and 2*),* and we optimized an LNP formulation for IV delivery with the desired biophysical properties: 80 nm in diameter, monodisperse, and high encapsulation efficiency (Supplementary Fig. 3a).

To ensure vRNA replication is initiated after polyprotein translation, the termini of the IVT vRNA must recapitulate those of the RNA viral genome encapsidated in the viral capsid. These termini are generated during IVT by an optimized 5’ ribozyme and runoff template produced by cleavage of a Type IIS restriction enzyme at the 3’ termini. To enhance the potency of the Synthetic-SVV, we optimized the vRNA by introducing modifications in the internal ribosome entry site (IRES)[19] and included a gain of function mutation in VP2 that improves viral entry[20], which improved replication and efficacy compared with the SVV-001 vRNA[21] (Supplementary Fig. 3b, c). Moreover, SVV replication was only detected in tumor cells and not in liver tissue (Supplementary Fig. 3d), further demonstrating that systemic distribution of the vRNA/LNP selectively initiates viral replication only in permissive tumor cells and not in healthy cells.

Intravenous administration of Synthetic-SVV inhibits tumor growth in an SCLC cancer model. Intravenous administration of 1 mg/kg Synthetic-SVV resulted in significant tumor growth inhibition (TGI) in the NCI-H446 SCLC xenograft model (Fig. 2a) and was well tolerated (Fig. 2b). Administration of Synthetic-SVV-Neg (a mutated SVV vRNA unable to initiate virus production) did not inhibit tumor growth, suggesting that the efficacy observed is associated with SVV vRNA replication. Moreover, 3 days after IV delivery of Synthetic-SVV, a robust fluorescent *in situ* hybridization (FISH) signal in the tumor was detected from both the positive and negative-sense RNA strands (Fig. 2c). Picornavirus replication starts with the synthesis of a negative-strand copy of the viral genome, which serves as a template for new vRNA or positive-strand RNA. Detection of the negative-strand unequivocally reveals viral replication and can be differentiated from the vRNA/LNP. In tumors treated with Synthetic-SVV, a greater signal for both strands

was observed relative to 1 x 10^6 PFU IV dose of SVV virions, indicating that Synthetic-SVV can trigger an infectious spread within the tumor that is as strong as the response achieved with live SVV IV treatment. In the tumors of mice dosed with Synthetic-SVV-Neg, only low levels of positive-strand RNA associated with blood vessels could be detected by FISH, most likely due to remaining vRNA/LNP.

The Synthetic vRNA platform is applicable to other picornaviruses. A second candidate, CVA21, was selected based on its oncolytic properties, favorable IV tolerability in cancer patients[22,23], and distinct tumor tropism compared to SVV[15,23]. We developed a Synthetic-CVA21 consisting of an IVT transcribed vRNA/LNP (Supplementary Fig. 1b, c). Similarly, an LNP formulation with desirable biophysical properties was achieved with CVA21 vRNA using the composition described for SVV vRNA (Supplementary Fig. 3a). Complete tumor regression at dose levels as low as 0.05 mg/kg was observed with Synthetic-CVA21 in the SK-MEL-28 melanoma model (Fig. 2d). Both dose levels tested (0.2 and 0.05 mg/kg) were also well tolerated, indicated by stable body weight and no adverse clinical signs (Fig. 2e). Transgenic mice expressing the human ICAM1 (huICAM1) gene, the cellular receptor for CVA21, recapitulate the expression of huICAM1 in mouse tissue and have been used as a biologically relevant model for the evaluation of CVA21 tolerability[24,25]. huICAM1 transgenic mice were used to evaluate the tolerability of 1 mg/kg IV administration of Synthetic-CVA21. Intravenous administration of Synthetic-CVA21 was well tolerated; no adverse clinical signs were observed up to 7 days after administration (Supplementary Fig. 4a). Histopathology was limited to mild microscopic liver findings, attributed primarily to the LNP. Low levels of CVA21 replication were detected by reverse transcription quantitative polymerase chain reaction (RT-qPCR) for CVA21 negative-strand and by plaque titer assay in spleen, liver, lung, heart, and kidney 2 days after injection. However, negative-sense RNA or CVA21 virions were undetectable at 7 days (Fig. 2f and Supplementary Fig. 4b), indicating that the mice had cleared CVA21 infection. These data suggest that Synthetic-CVA21 is tolerated in a mouse model sensitive to CVA21 at dose levels above those necessary to elicit tumor regression.

Synthetic RNA virus therapy is resistant to virus neutralizing antibodies. We postulated that the delivery of vRNA/LNP would be resistant to virus neutralizing antibodies in circulation. To test this hypothesis, we passively immunized immune-deficient mice with either a control rabbit serum or a rabbit anti- SVV serum with confirmed neutralization potency (Supplementary Fig. 5). Anti-tumor efficacy of either SVV virions or Synthetic-SVV in passively immunized mice bearing NCI-H466 tumors was compared (Fig. 3). SVV virions or Synthetic-SVV were administered intravenously on Days 1 and 8. Control serum treated animals dosed with SVV virions or Synthetic-SVV exhibited potent TGI relative to PBS. In the cohort of mice treated with the anti-SVV serum, IV administration of SVV virions was not efficacious for most animals. In contrast, Synthetic-SVV retained potent and lasting TGI in the group passively immunized with SVV neutralizing serum. These results demonstrate that, unlike live viruses, Synthetic-SVV is shielded from neutralizing antibodies and maintains anti-tumor activity.

IV administration of Synthetic-SVV leads to rapid kinetics of intratumoral viral replication. To explore the dose-response relationship after administration of Synthetic-SVV, we performed a dose titration analysis ranging from 0.2 to 0.025 mg/kg. Potent TGI in the NCI-H466 xenograft model was observed at all dose

levels; maximal TGI was observed at dose levels 0.1 mg/kg or above (Fig. 4a). Based on these data, 0.1 mg/kg was the dose selected to characterize the kinetics of viral replication after a single IV administration of Synthetic-SVV in NCI-H446 tumor-bearing mice. Tumors were harvested at multiple time points and analyzed by RT-qPCR and FISH. Viral negative-strand was detected by RT-qPCR as early as 1 day post treatment and reached a plateau in most tumors at 7 days post treatment. Remarkably, sustained SVV replication was detected up to 21 days after administering a single low dose of Synthetic-SVV (Fig. 4b). These findings were largely recapitulated with FISH detection of SVV positive and negative strands, with the FISH signal increasing to the maximum by Day 10 and spreading throughout the tumor bed at this timepoint (Fig. 4c).

Synthetic-SVV is efficacious in orthotopic SCLC and PDX models. In addition to the subcutaneously implanted xenograft models, which may be favorably exposed to LNP after IV administration due to the high vascularization of these models, we sought to evaluate Synthetic-SVV activity in a more challenging orthotopic small cell lung cancer (SCLC) model. SCLC is an appropriate indication for the clinical development of Synthetic-SVV, given SVV established tropism for tumors of neuroendocrine origin[15,21]. After confirming that the SCLC human cell line NCI-H82 was sensitive to SVV *in vitro* and *in vivo* (in a subcutaneous model, data not shown), the efficacy of Synthetic-SVV was assessed in a survival study. Lung orthotopic implantation of NCI-H82 cells in mice led to a median survival of 52 days in the PBS group (Fig. 5a). Synthetic-SVV administered on Days 15 and 22 after tumor implantation yielded a significant therapeutic benefit vs. control arms (Fig. 5a), with mice surviving a median of 100 days, nearly doubling survival in this model. In a parallel study, tumor burden was examined 10 days post-second treatment using hDLL3 immunohistochemistry (IHC). Significant reduction of tumor burden and extensive central tumor necrosis was observed in the lung of mice treated with Synthetic-SVV relative to Synthetic-SVV-Neg or PBS control (Fig. 5b, c).

Patient-derived xenograft (PDX) tumor models better represent the heterogeneity of human cancers[26]. Given that SCLC is known for its heterogeneity leading to recurrence and emergence of treatment resistant disease[27,28], we evaluated the ability of Synthetic-SVV to replicate in an SCLC PDX model. Mice were dosed systemically with Synthetic-SVV, Synthetic-SVV-Neg, or PBS and SVV virions intratumorally as a positive control. RT-qPCR of the SVV negative-strand showed that Synthetic-SVV achieved similar levels of viral replication to SVV virions despite being dosed intravenously (Fig. 5d). Furthermore, potent anti-tumor activity (TGI = 94% on Day 22) was observed after two weekly doses (Days 1 and 8) of Synthetic-SVV (Fig. 5e) compared to vehicle control and Synthetic-SVV-Neg.

Combination therapy with anti-PD-1 improved durable TGI in a syngeneic neuroendocrine tumor model. The mode of action of OVs involves the stimulation of anti-tumor immunity and the direct killing of cancer cells, which release potential tumor antigens in an inflamed TME[29]. These activities may be advantageous for treating SCLC and NSCLC, indications with high tumor mutational burden[30-32] and known to be sensitive to SVV and CVA21, respectively. To assess whether Synthetic RNA viruses can stimulate an immune response, SVV sensitive murine syngeneic neuroblastoma model, N1E-115[33], was

used. Tumor profiling of N1E-115 TME showed these tumors were poorly infiltrated by immune cells compared to other syngeneic mouse tumors (Supplementary Fig. 6). In this tumor model, administration of Synthetic-SVV led to a significant increase in the recruitment of CD8 T cells and a trend for CD4 T cells and NK cells in tumors (Fig. 6a and Supplementary Fig. 7a). Regulatory T cells (Treg) numbers were not increased in tumors, leading to an overall elevated CD8/Treg ratio that has been associated with improved clinical benefit to anti-PD-1[34](Fig. 6b). The CD8 T cells showed an activated phenotype, with upregulated CTLA4 and PD-1 (Fig. 6c). Both short-lived effector cells (SLEC) and memory precursor effector cells (MPEC) were increased with Synthetic-SVV compared with control (Fig 6d). Tumor-associated macrophages were also profiled, and an increased M1 (phagocytic)/M2 (proinflammatory) ratio was observed (Fig. 6e and Supplementary Fig. 7b). The number of M1 macrophages (Fig. 6f) and tumor cells expressing PD-1 ligand (PD-L1) were also significantly increased (Fig. 6g). These data indicate that Synthetic-SVV promotes a change within the TME conducive to anti-tumor immunity. Two weekly doses of Synthetic-SVV at 1 mg/kg led to significant TGI (Supplementary Fig. 8). Notably, due to the increased PD-1 and PD-L1 expression, the efficacy of Synthetic-SVV in combination with anti-PD-1 antibody in the N1E-115 model was evaluated. The TGI achieved with a suboptimal dose of synthetic SVV in this model was further enhanced when administered as combination therapy with anti-PD-1 antibody (Fig. 6h).

Discussion

This report describes the design and development of Synthetic RNA virus for the systemic treatment of cancer. Intravenous delivery of the vRNA genomes for 2 picornaviruses, SVV and CVA21, formulated in LNPs, are well tolerated and promote tumor-specific production of OVs and initiation of both immune cell recruitment and tumor destruction. Efficacy was observed in multiple cancer models, including xenografts, PDX, and syngeneic models. Moreover, Synthetic-SVV improves survival in an orthotopic SCLC tumor model. Most importantly, Synthetic-SVV remains efficacious even in the presence of circulating virus-specific neutralizing antibody and was further potentiated by the combination with an immune checkpoint inhibitor (ICI) anti-PD-1 antibody.

Clinical stage OVs, including those with no prior exposure in humans such as enadenotucirev, a non-naturally occurring adenovirus, have reported neutralization after repeated IV dosing, likely limiting the therapeutic window of effectiveness of the viral immunotherapy to a short time period[15,16,35]. Other OVs, such as CVA21 and reovirus, also have reported the presence of neutralizing antibodies after systemic administration[22,36]. Patisiran, a LNP-based formulation of a siRNA, rarely elicits anti-drug antibodies[37]. Thus, we expect a similar response with the IV administration of Synthetic RNA viruses and do not anticipate any scheduling limitation with this treatment approach.

We enabled 2 picornaviruses for this platform, and are we are currently adapting it for additional RNA viruses. This approach is anticipated to overcome the central challenge of OVs repeat IV administration by evading neutralization of the therapeutic agent by the humoral response. Intratumoral administration of OVs is clinically effective but is generally limited to patients with injectable tumors[2]. To date, evidence

of clinical benefit has primarily been observed in cutaneous malignancies[38]. Efficacy of OVs in metastatic disease following intra-lesional injections requires a systemic immune response to overcome the immunosuppressive environment of the non-injected tumors, which might be limited to some indications such as melanoma, which are primed to respond to immune intervention[39]. Therefore, systemic administration must be achieved to effectively deploy viral immunotherapies to treat patients with various cancer types, including lung cancer, where safe, repeat intra-lesional injections have been challenging to accomplish.

SVV has a well-described tropism for SCLC[16,21], as confirmed by our data showing anti-tumor activity and survival benefit in cancer models. CVA21 tumor tropism is driven by the expression of its entry receptor ICAM1, which is highly expressed in NSCLC and other tumor indications[40,41]. In addition to its entry receptor, viral tropism is also dictated by a range of viral restriction factors within the infected cell, which are essential to consider in the context of the Synthetic RNA virus delivery platform, which uses LNP to initially bypass the viral entry receptor. LNP formulations for SVV and CVA21 yield small nanoparticles (average of 80 nm) and are slightly negatively charged. These properties make them adequate for avoiding phagocytosis by tissue-resident macrophages and diffusing through tissues[42,43]. Despite the systemic distribution of Synthetic RNA virus, minimal to no detection of SVV or CVA21 replication was observed in normal mouse tissues. Furthermore, we assessed CVA21 replication and viral production following IV dosing in huICAM1 transgenic mice, which are sensitive to CVA21 infection[44]. These results support tumor selectivity of Synthetic RNA virus replication and their elimination by host anti-viral response in normal tissues, which suggests that this modality will achieve an acceptable tolerability and an appropriate therapeutic window as observed in our preclinical models.

The activity of OVs is mediated by a dual mode of action, which involves the direct oncolysis of tumor cells and the stimulation of anti-tumor immunity, facilitating the release of tumor antigens and the detection of viral replication leading to immune cells recruitment and activation[45]. The potent anti-tumor activity and survival benefit of Synthetic RNA virus in human tumor models xenografted in immunocompromised mice are likely due to the unconstrained spread of infection within the tumor and subsequent oncolysis. In an immunocompetent host, the infection may likely be limited by immune cells recognizing and eliminating infected cells, which may contribute to the efficacy of Synthetic RNA virus. In a syngeneic tumor model sensitive to SVV, Synthetic-SVV increased the number of CD8 T cells and M1 phagocytic macrophages, as generally observed for OVs[29,39,46]. Upregulation of PD-L1 on tumor and myeloid cells provided the rationale for the combination of Synthetic-SVV with anti-PD-1, which demonstrated an improved therapeutic benefit above the monotherapy. ICIs are approved for the treatment of SCLC and NSCLC, but the benefits are limited to a small percentage of patients. In metastatic melanoma, treatments with ICI and OVs are currently being evaluated in the clinic[39,46-48]. Combination therapy of ICI and Synthetic RNA viruses could increase the success of both therapies for lung cancers.

The Synthetic RNA virus platform is a novel therapeutic modality for cancer treatment that can enhance the oncolysis and immune-stimulating activity of OVs while providing the convenience of repeat IV administration of vRNA formulated in LNP. Both Synthetic-SVV and

-CVA21 have potent activity in preclinical models, even in the presence of neutralizing

antibodies, and are well tolerated. These data support the progression of Synthetic-SVV and -CVA21 to clinical trials for the treatment of lung cancer and other permissive tumor indications as monotherapy or in combination with standard of care ICIs.

Online Methods

Cell lines

Cell lines NCI-H466 (HTB-171), NCI-H82 (HTB-175), NCI-H1299 (CRL-5803), SK-MEL-28 (HTB-72), CT26 (RL-2638), 4T1 (CRL-2539), and N1E-115 (CRL-2263) were all purchased from ATCC (Gaithersburg, MD). CT-2A-luc (SCC195) and MCC14/2 (10092303) were purchased from Millipore Sigma (Burlington, MA). Murine colon adenocarcinoma cell line MC38 was kindly donated by Prof. Joseph Glorioso from the University of Pittsburgh.
NCI-H446, NCI-H82, NCI-H1299, SK-MEL-28, MCC14/2, CT26, and 4T1 cell cultures were all maintained in RPMI-1640 medium (Gibco, Gaithersburg, MD) supplemented with 10% heat-inactivated FBS (Gibco, Gaithersburg, MD) and 1% penicillin/streptomycin (Gibco, Gaithersburg, MD). MC38, CT-2A-luc, and N1E-115 cells were cultured in DMEM medium (Gibco, Gaithersburg, MD) supplemented with 10% heat-inactivated FBS and 1% penicillin/streptomycin. All cell cultures were incubated in a humidified atmosphere with 5% CO_2 at 37˚C.

IVT template design and construction

Picornaviral positive-strand sequences were obtained from NCBI (SVV-001[49] (GenBank: DQ641257) and CVA21[50] (Genbank: AF546702.1). Custom ribozymes were designed for the 5’ of the viral template, and 30 nucleotide poly adenosine (pA) sequences were added to the 3’ end, followed by either SapI (SVV) or BsmBI (CVA21) restriction site to generate polythymidine templates of the appropriate length after linearization. SVV IRES2 sequence corresponds to SVA/Canada/MB/NCFAD-104-1/2015 (GenBank: KY486156). The IVT templates were constructed with synthetic dsDNA fragments (IDT Geneblocks, Genscript, Piscataway, NJ) and Gibson assembly (NEBuilder HiFi DNA Assembly Master Mix, Catalog #E2621L, NEB, Ipswich, MA) following the manufacturer protocol. These constructs were sequenced end to end, linearized with either SapI (SVV) or BsmBI (CVA21) (NEB SapI # R0569L, BsmBI # R0739L, Ipswich, MA), and research-grade IVTs (NEB HiScribe T7 High Yield RNA Synthesis Kit Catalog #E2040S, Ipswich, MA) were performed to ensure viral kickoff. All viral stocks used in this work were obtained with these reverse genetics systems.

IVT and LNP formulation

Large scale IVTs (20-100 mg) were performed at Aldevron (Fargo, ND) and purified by diafiltration. In some instances, IVTs (1-50 mL) were performed internally using a heating block (Eppendorf Thermomixer, Hamburg, Germany) at 37°C for 2.5 h using a buffer containing magnesium acetate, Tris-HCl (EMD-Millipore, Danvers, MA), TCEP (EMD Millipore Danvers, MA), equimolar NTPs (Thermo Fisher Scientific, Waltham, MA), inorganic pyrophosphatase (NEB Ipswich, MA), and T7 RNAP (NEB, Ipswich, MA). DNase I (NEB, Ipswich, MA) was added at the end of the IVT for 30 minutes and quenched with EDTA (Thermo Fisher Scientific, Waltham, MA). Next, tangential flow filtration (TFF) was performed using a 100 kDa mPES membrane (Repligen, Marlborough, MA) and diafiltered using water. The TFF retentate was subsequently salt adjusted and loaded onto an Oligo-dT chromatography column (BIA Separations, Ajdovščina, Slovenia). RNA containing a pA tail was eluted using water. A final TFF step was performed as a desalting step to ensure the desired RNA concentration (1.0 mg/mL) and pH (6.5) were achieved. These RNAs were the basis for LNP generation.

LNPs were prepared by mixing appropriate volumes of lipids in ethanol with a vRNA containing aqueous phase using a NanoAssemblr (Precision NanoSystems) microfluidic device followed by downstream processing. Using a flow ratio of 3:1 aqueous:organic phase, the solutions were combined using a microfluidic chip and a total flow rate of 12 mL/min. LNPs were dialyzed against a neutral pH buffer such as 1X PBS to remove ethanol and raise the pH. The resulting LNPs were concentrated using Amicon Ultra centrifugal filter units with 100,000 Da molecular weight cut-off (Millipore, Burlington, MA). RNA encapsulation was assayed using Quant-iT RiboGreen (Thermo Fischer Scientific, Waltham, MA) and a microplate reader (SpectraMax, San Jose, CA). Hydrodynamic size and PDI of the LNPs were analyzed by dynamic light scattering using a Zetasizer Nano ZS (Malvern Panalytical, Malvern, United Kingdom).

vRNA transfection, infection and viral stock production

Viral stock production was done by vRNA transfection using Lipofectamine RNAiMax® (Thermo Fisher Scientific, Waltham, MA). Transfection reagent (1µg/ml) was added to NCI-H1299 cells seeded in a 12-well tissue culture plate at 1 x 10^5 cells/well. After 72 h post-transfection, supernatants were collected, centrifuged at 2000xg for 5 minutes, and filtered through a 0.45-micron filter. Filtered supernatant (100 µl) was used to infect a new 12-well plate seeded with NCI-H1299 cells. After 72 h, cells and supernatants were subjected to 3X freeze-thaw cycles, then centrifuged and filtered. Supernatant (1 mL) was then used to infect NCI-H1299 cells grown to 80% confluency in a two-chamber CellSTACK® (Corning, Corning, NY) tissue culture vessel in 250 ml of growth media. After 96 h post-infection, the cells and supernatants were 3X freeze-thawed, centrifuged, filtered, and concentrated using 100K Amicon® Ultra 15 Centrifugal Filter Units (Millipore, Burlington, MA) to a 10 ml final volume which was aliquoted and stored at -80 C.

Viral plaque titers and IC_{50} protocols

To quantify SVV infectivity by IC_{50} NCI-H446 cells were seeded into 96-well tissue culture plates at 1 x 10^4 cells/well and incubated at 37°C, 5% CO_2. After 48 h, culture medium was aspirated and replaced with 10-fold serial dilutions of infectious SVV in a 100 µL volume. After 48 h, cell viability of infected or mock-treated cells was measured with CellTiter-Glo® luminescent assay (Promega, Madison, WI) using a

microplate reader (Molecular Devices, SpectraMax i3X minimax imaging cytometer, San Jose, CA). Raw data was converted to percentage survival relative to mock-infected. Values were graphed in GraphPad Software Prism 9.0 and analyzed using a non-linear sigmoidal plot with variable slope (asymmetric four-point linear regression) to generate IC_{50} values. For each sample, at least five technical were analyzed to calculate IC_{50}.

To quantify SVV virus titer by plaque assay, 2 x 10^5 MCC14/2 cells/well were seeded into 12-well tissue culture plates. After 24 h, infectious virus was 10-fold serially diluted in serum-free media. Culture media from the cells was aspirated and replaced with 300 µL/well of diluted virus for an adsorption period of 1 h at 37°C with gentle rocking. Virus samples were analyzed in technical triplicate. Post adsorption, 2 mL of pre-warmed 1% methylcellulose in media with 5% FBS was added to each well. After 48 h, wells were aspirated and stained with crystal violet solution. Discrete plaque-forming colonies were counted manually to determine titer.

To quantify CVA21 virus by plaque assay, 2 x 10^5 SK-MEL28 cells/well were seeded in a 24-well plate (or 2.5 x 10^5 NCI-H1299 cells/well in a 12 well plate). Mouse tissue homogenates were produced by resuspending pulverized frozen tissue samples in 2 µl PBS/mg of tumor. After mixing, samples were pelleted, and supernatants were recovered. Whole tissue homogenates were 10-fold serially diluted in serum-free media. After media was removed, 250 µl of the dilutions were added to each well. The plate was gently rocked at 37 C for 1 hr. Then, 1 ml of pre-warmed 1% methylcellulose in 5% FBS containing media was added as an overlay. Plates were incubated for 48 hr prior to adding 250 µl crystal violet stain to each well; afterwards, the overlay was removed and rocked at room temperature for 30 min. The plates were washed and allowed to dry to visualize plaques.

SVV antisera and neutralization assay

Polyclonal rabbit SVV antisera were generated against UV-inactivated SVV at Maine Biotechnology Services (Portland, ME). To measure the neutralization titer, NCI-H446 cells were seeded into 96-well tissue culture plates at 1 x 10^4 cells/well in complete media and incubated at 37°C, 5% CO_2. After 48 hr, 1 x 10^7 $TCID_{50}$/mL of SVV was mixed with rabbit anti-SVV sera diluted in complete media. Serial two-fold dilutions of sera from 1:20 to 1:5120 were tested. Culture media was aspirated from the cells and replaced with 100 µl of diluted SVV per well. Cells were returned to incubation at 37°C, 5% CO_2, and *in vitro* viability assays were performed at 48 h post-infection by adding 100 µL/well of CellTiter-Glo® 2.0 reagent (Promega, Madison, WI). Total luminescence (RLU) was measured on a plate reader (Molecular Devices, SpectraMax i3X minimax imaging cytometer, San Jose, CA). Raw data were converted to percentage survival relative to mock-infected, and values were graphed in GraphPad Software Prism 9.0.

Mice, tumor models, and treatment

Studies in xenografts and syngeneic tumor models

In vivo experiments in xenograft tumor models NCI-H466, NCI-H82, NCI-H1299, and SK-MEL-28 were conducted in 8–12-week-old NU/NU nude female mice (Charles River Laboratories, Wilmington, MA). N1E-115 murine neuroblastoma tumor model was established in 8–12-week-old A/J female mice (The Jackson Laboratory, Bar Harbor, ME). For studies in 4T1 and CT26 tumor models, 8–12-week-old female BALB/c mice (Charles River Laboratories) were used. Studies using the MC38 and CT-2A-luc tumor model were conducted in 8–12-week-old female C57BL/6 mice (Charles River Laboratories). All animals had unlimited access to a sterile, pelleted rodent diet and reverse osmosis-purified water and were maintained on a 12:12-h light:dark cycle with access to environmental enrichment. All animal protocols were approved by the Oncorus Institutional Animal Care and Use Committee (IACUC) and were performed in accordance with IACUC regulations. To establish subcutaneous xenograft tumor models, 5 x 10^6 – 1 x 10^7 viable tumor cells were injected into the right flank of nude mice in 100 µl of Matrigel (Corning, Glendale, AZ):PBS (Gibco, Gaithersburg) mixture (1:1 v/v).

For the subcutaneous syngeneic N1E-115 tumor model, viable 5 x 10^5 N1E-115 cells were injected in 100 µl of Matrigel in PBS mixture (1:1 v/v) into the right flank of A/J mice. For the subcutaneous MC38 tumor model, viable 5 x 10^5 MC38 cells were injected in 100 µl of PBS into the right flank of C57BL/6 mice. Murine breast cancer (4T1) and colon carcinoma (CT26) models were established in BALB/c mice by subcutaneous injection of 1 x 10^6 cells in 100 µl of PBS into the right flank of the animals. Treatment was initiated when tumors reached the pre-determined volume of 150 ± 30 mm^3 for human xenograft models and 100 ± 25 mm^3 for syngeneic tumors. Animals were pair-matched based on tumor volume and randomly assigned to treatment arms. Synthetic-SVV was dosed intravenously at doses ranging from 0.025 to 1.0 mg/kg at weekly intervals for a total number of up to 4 doses, as explained in figure legends. For combination therapy, the anti-mPD-1 antibody (Clone RMP1-14, Bio X Cell, Lebanon, NH) was dosed intraperitoneally (IP) at a fixed dose of 200 µg/animal, every third day, for a total of 3 doses. Animals on treatment were observed daily for clinical manifestations of adverse events, body weight, and tumor volumes were recorded biweekly. Tumor volume was calculated using the following formula: $V = a \times b^2/2$, where a is longer diameter and b is shorter diameter. Mice were humanely euthanized once tumor burden reached 2000 mm^3.

For the orthotopic SCLC tumor model, viable 5 x 10^6 NCI-H82 cells suspended in Matrigel:PBS mixture (1:1 v/v) were implanted into the left lung lobe via intra-thoracic injection. Treatment commenced 2 weeks post-orthotopic cell inoculation and consisted of 2 1.0 mg/kg IV doses of Synthetic-SVV-Neg or Synthetic-SVV administered 7 days apart. For survival analysis, mice were observed for pre-determined survival endpoints, which in the case of orthotopic lung tumors comprised of symptoms of lung disease and decreased body conditions (i.e., body weight loss exceeding 20%).

Orthotopic CT-2A-luc mouse glioma tumors were established in 11-12 weeks old female C57BL/6 mice by intracerebral injection of 5 x 10^4 CT-2A-luc cells suspended in 2 µl of PBS. Tumors were allowed to grow for 14 days, then mice were humanely euthanized, tumors were collected, enzymatically dissociated and immunophenotyped as described below. **Immunohistochemical analysis of orthotopic tumor burden**

Lungs were collected from treated animals 10 days post-second Synthetic-SVV dose and were fixed in 10% buffered formalin for 24 h, paraffin processed, and sectioned at the level of mainstem bronchi. For IHC detection of DLL3, sections were stained with rabbit antibody specific to human DLL3 (Clone E3J5R, Cell Signaling Technology, Danvers, MA), digitally scanned, and subjected to morphometric analysis using QuPath software.

Efficacy of Synthetic-SVV in mice passively immunized to SVV

Nude mice with subcutaneous NCI-H446 tumors were passively immunized to SVV by intra-peritoneal injection of 1.5 mg of rabbit SVV anti-serum. Control animals received a corresponding amount of normal rabbit serum (Normal Rabbit Serum, ImmunoReagents, Inc., Raleigh, NC). Immunization cycle was repeated twice 7 days apart. After 24 h post each adoptive serum transfer, control and passively immunized mice were intravenously treated with either 10^6 PFU of SVV virions or 1.0 mg/kg Synthetic virus.

Synthetic-CVA21 tolerability in hICAM1 transgenic mice

Tolerability was assessed in CVA21-permissive huICAM1 transgenic mice after a single IV dose of Synthetic-CVA21 1.0 mg/kg. Animals were observed daily for clinical symptoms of adverse events and weighed for 5 consecutive days following treatment. Tissue pathology and CVA21 replication in treated animals were evaluated at 2- and 7-days post-treatment.

Efficacy of Synthetic-SVV in SCLC PDX model

To establish the SCLC PDX model, 2 x 2 mm fragments of LU5184 SCLC tumors (Crown Bioscience, San Diego) were implanted using a sterile trocar into 6–8-week-old female NOD SCID mice (The Jackson Laboratory, Bar Harbor, ME). Treatment commenced once tumors reached a pre-determined volume of approximately 150 mm^3 ± 50 mm^3. Animals were pair-matched based on tumor volume and randomly assigned to treatment groups. Synthetic-SVV and Synthetic-SVV-Neg were dosed in 2 intravenous 1.0 mg/kg doses administered at weekly intervals. Animals on treatment were observed daily for clinical manifestations of adverse events, body weight, and tumor volumes were recorded biweekly. Mice were humanely euthanized once tumor burden reached 3000 mm^3. For the pharmacodynamic analysis of virus replication in SCLC PDX tumors, tumor-bearing mice were treated with a single, intravenous dose of 1 mg/kg Synthetic-SVV or Synthetic-SVV-Neg. Five days post-treatment, tumors were collected and processed to evaluate negative-strand SVV RNA by RT-qPCR. Another group of mice was treated with 2 intratumor doses of 10^6 PFU SVV virions on Days 1 and 3. Two days post-second treatment, tumors were collected and processed to evaluate negative-strand SVV RNA by RT-qPCR.

SVV and CVA21 RNA negative-strand specific RT-qPCR

Tumor RNA extraction

Tumor samples were kept frozen during the entire procedure preceding RNA extraction using dry ice and liquid nitrogen to flash freeze. Samples were pulverized using Cp02 cryoPREP Automated Dry Pulverizer (Covaris, 500001, Covaris, Woburn, MA) for SVV- and CVA21-treated tumor samples. For SVV samples, 10 mg of pulverized sample was weighed and transferred to a 2 mL microcentrifuge tube (Sample Tube RB, QIAGEN 990381, Hilden, Germany). Buffer RLT Plus with B-mercaptoethanol (600 µL) was added to each sample and lysed. The remaining steps were performed using the QIAcube (QIAGEN, Hilden, Germany), following manufacturer's protocol for QIAGEN RNeasy Plus Mini Kit (QIAGEN 74134) under the section for Purification of Total RNA from Animal Tissues. RNA samples were treated with DNAseI (RNAse-free) (New England Biolabs, #M0303S, Ipswich, MA) after extraction.

For CVA21 samples, 10 mg of pulverized sample was weighed and transferred to a 1.5 mL microcentrifuge tube. Lysis Buffer/Proteinase K mixture (400 µL) (RNAdvance Tissue Kit, Beckman Coulter, A32649, Pasadena, CA) was added to each sample. Samples were incubated at 37°C for at least 30 min to lyse samples completely. The remaining steps were performed using the Biomek i5 (Beckman Coulter, B87583, Pasadena, CA) following manufacturer's protocol (RNAdvance Tissue Kit). The RNAdvance Tissue Kit includes a DNase I treatment step.

cDNA synthesis and quantitative PCR analysis

RNA samples were normalized to an equal input for cDNA synthesis. Virus negative-strand specific primers were used to synthesize cDNA. The SVV negative-strand specific primer 5'-GCGCAAATTCGTCCAAAACAACGAC-3' and the CVA21 negative-strand specific primer 5'-AGACTACGGACTGACCATGACTC TTAGGACGCTTTTACTGAGAAC -3' were synthesized by Integrated DNA Technologies (IDT, Coralville, Iowa). For both SVV and CVA21, cDNA synthesis was performed using SuperScript IV First-Strand Synthesis System (Invitrogen, 18091200, Carlsbad, CA) and their respective specific primers.

Quantitative PCR (qPCR) analysis was performed using TaqMan probe chemistry. qPCR reactions (20 µL) were made containing 10 µL of TaqMan Fast Advanced Master Mix (Applied Biosystems, 4444557, Foster City, CA), 1 µL of TaqMan Gene Expression Assay, FAM probe (Applied Biosystems, 4332078), 4 µL of nuclease-free water, and 5 µL of diluted cDNA. TaqMan Gene Expression Assay probes were made customized for either SVV or CVA21. SVV probe 5'-TGGAAGCCATGCTCTCCTACTTCA-3', forward primer 5'-CGACGGCTTATACAAACCAGTTA-3', reverse primer 5'-AGCTTCTCGAGTAGTGTTCCT-3' and CVA21 probe 5'-TGCCTATGGTGATGACGTGATAGCT-3', forward primer 5'- GAGAACCTACAAGGGCATAGAC-3', and reverse primer 5'- TAGGAGACTAGCGTCAACCT-3' were custom ordered through Applied Biosystems (ThermoFisher Scientific, Waltham, MA). qPCR parameters 95°C for 20 s followed by 40 cycles at 95°C for 1 s and 60°C for 30 s. Each qPCR assay contained technical triplicates for each standard and sample.

SVV fluorescent *in-situ* hybridization

Tumors were harvested at the indicated timepoints, bisected, fixed in 10% buffered formalin for 24 h at room temperature, and paraffin-embedded. RNAscope FISH of SVV negative and positive RNA strand was performed at Advanced Cell Diagnostics (ACD, Newark, CA). Standard RNAscope LS Multiplex fluorescent pretreatment conditions were used. Briefly, epitope retrieval was performed at 15 min at 95˚C, followed by protease III treatment for 15 min at 40˚C. Samples were first evaluated for quality using the positive and negative reference controls for specificity and sensitivity (ACD Catalog # 313908 and 320758, respectively). Custom SVV probes were designed for both the positive and negative strands (ACD Catalog # 819848 and 819858-C2, respectively) and were confirmed to be specific. All of the samples passed QC with positive control staining, and little to no background staining was observed. RAW data was analyzed with 3DHISTECH CaseViewer Software (3DHISTECH Ltd, Budapest, Hungary).

Immune profiling of tumors

For flow cytometry, tumors were collected on Day 14 after the first dose. Tumors were weighed and then cut into small pieces before being disaggregated into single-cell suspensions using a Miltenyi GentleMACs Octo-dissociator with heaters according to manufacturer's instructions. A T/NK cell and a myeloid cell flow panel were performed using the following reagents and Ab clones: A LIVE/DEAD™ Fixable Red Dead Cell Stain Kit for 488 nm excitation (Invitrogen, Catalog # L32102) was used to assess the viability. Surface cell staining was performed by using BD Stain Buffer (Becton-Dickinson Catalog # 554656) with the antibodies for mouse CD45 (30-F11, Catalog # 103154), CD3e (17A2, Catalog # 100218), CD8a (53-6.7, Catalog # 100730), CD4 (RM4-5, Catalog # 100552), CD25 (PC61, Catalog # 102041) CD69 (REA937, Catalog # 130-115-461), CTLA-4 (UC10-4B9, Catalog # 106323), NKP46 (29A1.4, Catalog # 137612), KLRG1 (2F1, Catalog # 138409), CD127 (A7R34, Catalog # 135035), PD-1 (29F.1A12, Catalog # 135216), MHCII (M5/114.15.2, Catalog # 107635), Ly6C (H,1.4, Catalog # 128037), CD206 (C068C2, Catalog # 141720), CD86 (GL-1, Catalog # 105037) and PD-L1 (10F.9G2, Catalog # 124312). Foxp3/Transcription Factor Staining Buffer Set (eBioscience Catalog # 00-5523-00) was used for FOXP3 (150D, Catalog # 320008) and CTLA-4 (UC10-4B9, Catalog # 106323) intracellular staining. All antibodies were purchased from BioLegend (San Diego, USA), except CD69 Miltenyi Biotech (Bergisch Gladbach, Germany). Data were acquired on a BD LSRFortessa using BD FACSDiva software and analyzed using FlowJo software. For the T cell and NK panel, cells were first gated for time (SSC-A vs. Time), lymphocytes (SSC-A vs. FSC-A), and singlets (FSC-H vs. FSC-A). The lymphocyte gate was further analyzed for their uptake of the Live/Dead stain to determine live vs. dead cells and CD45 expression. Then, the cells were gated on CD3 vs. NKP46 to select T cells or NK cells. For the T cells, the population was gated for CD4 vs. CD8, and the CD4 T cells were further gated for CD25+ and FOXP3+ to analyze the Treg population. NK cells were gated for NKP46+ and CD3-. For the myeloid panel, cells were first gated for time (SSC-A vs. Time) then lymphocytes (SSC-A vs. FSC-A), and singlets (FSC-H vs. FSCA). The lymphocyte gate was further analyzed for their uptake of the Live/Dead stain to determine live vs. dead cells and CD45 expression. Then, macrophages were gated using SSC-A vs. CD11b+ and subsequently on MHCII+Ly6C-subset. To distinguish between M1 and M2 macrophages, we used CD206-CD86+ for M1 and CD206+CD86- for M2. Enumeration of cells per mg of tumor was calculated using 123Count eBeads (Invitrogen, Catalog # 01-1234-42, Carlsbad, CA). A fixed volume of beads with a known concentration

was added to each well prior to analysis by flow cytometry. The number of beads in the gated fraction was then used to calculate cell number using the following equation:

$$Absolute\ count\ \left(\frac{cells}{\mu L}\right) = \frac{(cell\ count\ x\ eBead\ volume)}{eBead\ count\ x\ cell\ volume)} \times\ eBead\ concentration$$

Declarations

Acknowledgments

This study was sponsored by Oncorus, Inc. The authors acknowledge and thank Sofie Denies

for statistical analysis, James B. Rottman (Athenaeum Pathology Consulting) for

morphometric analysis. The authors also thank Chastity Bradley, PhD of BioMed Writers, LLC, for her editorial review of the manuscript and assistance with manuscript submission.

Author Contributions

Conceptualization:

E.M.K., M.F., C.Q., L.L.

Methodology:

E.M.K., A.D., J.H., L.K., A.D.A., J.B., J.S.L., J.J., S.F., M.H., E.L.M., A.R., L.H., D.D., J.S., S.A., J.D., M.S., B.B.H., C.Q., L.L.

Software:

E.M.K., A.D., J.S.L., S.F.

Validation:

E.M.K., A.D., J.H., L.K., A.D.A., J.B., J.S.L., J.J., S.F., M.H., E.L.M., A.R., L.H., D.D., J.S., S.A., J.D., M.S

Formal Analysis:

E.M.K., A.D., J.B., J.S.L., J.J., S.F., B.B.H., C.Q., L.L.

Writing – Review & Editing:

E.M.K., A.D., A.D.A., J.B., J.S.L., S.F., J.D., M.S., B.B.H., T.A, C.Q., L.L.

Supervision:

E.M.K., A.D., S.F., B.B.H., C.Q., L.L.

Project Administration:

E.M.K., C.Q., L.L.

Approval of final draft: E.M.K., A.D., J.H., L.K., A.D.A., J.B., J.S.L., J.J., S.F., M.H., A.R., L.F., D.D., J.S., S.A., J.D., M.S., B.B.H., T.A, M.F., C.Q., L.L.

Data availability

The data that support the findings of this study are available from the corresponding author upon request.

Conflict of Interest

E.M. Kennedy, A. Denslow, J. Hewett, L. Kong, A. De Almeida, J. Bryant, J.S. Lee, J. Jacques, S. Feau, M. Hayes, E.L. McMichael, A. Rhameh (at the time the study was conducted), L. Herschelman (at the time the study was conducted), D. Douglas (at the time the study was conducted), J. Spinale, S. Adhikari, J. Deterling, M. Scott, B.B. Haines, T. Ashburn, C. Quéva, L. Lerner are all employees of Oncorus, Inc. No other authors have any conflicts of interest to disclose.

References

1 Andtbacka, R. H. *et al.* Talimogene Laherparepvec Improves Durable Response Rate in Patients With Advanced Melanoma. *J Clin Oncol* **33**, 2780-2788, doi:10.1200/JCO.2014.58.3377 (2015).

2 Zheng, M., Huang, J., Tong, A. & Yang, H. Oncolytic Viruses for Cancer Therapy: Barriers and Recent Advances. *Mol Ther Oncolytics* **15**, 234-247, doi:10.1016/j.omto.2019.10.007 (2019).

3 Martinez-Quintanilla, J., Seah, I., Chua, M. & Shah, K. Oncolytic viruses: overcoming translational challenges. *J Clin Invest* **129**, 1407-1418, doi:10.1172/JCI122287 (2019).

4 Yamamoto, Y., Nagasato, M., Yoshida, T. & Aoki, K. Recent advances in genetic modification of adenovirus vectors for cancer treatment. *Cancer Sci* **108**, 831-837, doi:10.1111/cas.13228 (2017).

5 Menotti, L. *et al.* HSV as A Platform for the Generation of Retargeted, Armed, and Reporter-Expressing Oncolytic Viruses. *Viruses* **10**, doi:10.3390/v10070352 (2018).

6 Franco-Luzon, L. *et al.* Systemic oncolytic adenovirus delivered in mesenchymal carrier cells modulate tumor infiltrating immune cells and tumor microenvironment in mice with neuroblastoma. *Oncotarget* **11**, 347-361, doi:10.18632/oncotarget.27401 (2020).

7 Berkeley, R. A. *et al.* Antibody-Neutralized Reovirus Is Effective in Oncolytic Virotherapy. *Cancer Immunol Res* **6**, 1161-1173, doi:10.1158/2326-6066.CIR-18-0309 (2018).

8 Choi, J. W., Lee, Y. S., Yun, C. O. & Kim, S. W. Polymeric oncolytic adenovirus for cancer gene therapy. *J Control Release* **219**, 181-191, doi:10.1016/j.jconrel.2015.10.009 (2015).

9 Brugada-Vila, P. *et al.* Oligopeptide-modified poly(beta-amino ester)s-coated AdNuPARmE1A: Boosting the efficacy of intravenously administered therapeutic adenoviruses. *Theranostics* **10**, 2744-2758, doi:10.7150/thno.40902 (2020).

10 Tesfay, M. Z. *et al.* PEGylation of vesicular stomatitis virus extends virus persistence in blood circulation of passively immunized mice. *J Virol* **87**, 3752-3759, doi:10.1128/JVI.02832-12 (2013).

11 Wang, Y. *et al.* Liposome Encapsulation of Oncolytic Virus M1 To Reduce Immunogenicity and Immune Clearance in Vivo. *Mol Pharm* **16**, 779-785, doi:10.1021/acs.molpharmaceut.8b01046 (2019).

12 Aoyama, K. *et al.* Liposome-encapsulated plasmid DNA of telomerase-specific oncolytic adenovirus with stealth effect on the immune system. *Sci Rep* **7**, 14177, doi:10.1038/s41598-017-14717-x (2017).

13 Roberts, T. C., Langer, R. & Wood, M. J. A. Advances in oligonucleotide drug delivery. *Nat Rev Drug Discov* **19**, 673-694, doi:10.1038/s41573-020-0075-7 (2020).

14 Weng, Y. *et al.* Improved Nucleic Acid Therapy with Advanced Nanoscale Biotechnology. *Mol Ther Nucleic Acids* **19**, 581-601, doi:10.1016/j.omtn.2019.12.004 (2020).

15 Burke, M. J. Oncolytic Seneca Valley Virus: past perspectives and future directions. *Oncolytic Virother* **5**, 81-89, doi:10.2147/OV.S96915 (2016).

16 Schenk, E. L. *et al.* A Randomized Double-Blind Phase II Study of the Seneca Valley Virus (NTX-010) versus Placebo for Patients with Extensive-Stage SCLC (ES SCLC) Who Were Stable or Responding after at Least Four Cycles of Platinum-Based Chemotherapy: North Central Cancer Treatment Group (Alliance) N0923 Study. *J Thorac Oncol* **15**, 110-119, doi:10.1016/j.jtho.2019.09.083 (2020).

17 Hamid, O., Ismail, R. & Puzanov, I. Intratumoral Immunotherapy-Update 2019. *Oncologist* **25**, e423-e438, doi:10.1634/theoncologist.2019-0438 (2020).

18 Annels, N. E. *et al.* Phase I Trial of an ICAM-1-Targeted Immunotherapeutic-Coxsackievirus A21 (CVA21) as an Oncolytic Agent Against Non Muscle-Invasive Bladder Cancer. *Clin Cancer Res* **25**, 5818-5831, doi:10.1158/1078-0432.CCR-18-4022 (2019).

19 Xu, W. *et al.* Genome wide analysis of the evolution of Senecavirus A from swine clinical material and assembly yard environmental samples. *PLoS One* **12**, e0176964, doi:10.1371/journal.pone.0176964 (2017).

20 Cao, L. *et al.* Seneca Valley virus attachment and uncoating mediated by its receptor anthrax toxin receptor 1. *Proc Natl Acad Sci U S A* **115**, 13087-13092, doi:10.1073/pnas.1814309115 (2018).

21 Reddy, P. S. *et al.* Seneca Valley virus, a systemically deliverable oncolytic picornavirus, and the treatment of neuroendocrine cancers. *J Natl Cancer Inst* **99**, 1623-1633, doi:10.1093/jnci/djm198 (2007).

22 Pandha, H. *et al.* Abstract CT115: Phase 1bKEYNOTE 200 (STORM study):A study of an intravenously delivered oncolytic virus, Coxsackievirus A21 in combination with pembrolizumab in advanced cancer patients. *Cancer Research* **77**, CT115-CT115, doi:10.1158/1538-7445.Am2017-ct115 (2017).

23 McCarthy, C., Jayawardena, N., Burga, L. N. & Bostina, M. Developing Picornaviruses for Cancer Therapy. *Cancers (Basel)* **11**, doi:10.3390/cancers11050685 (2019).

24 Dufresne, A. T. & Gromeier, M. A nonpolio enterovirus with respiratory tropism causes poliomyelitis in intercellular adhesion molecule 1 transgenic mice. *Proc Natl Acad Sci U S A* **101**, 13636-13641, doi:10.1073/pnas.0403998101 (2004).

25 Hadac, E. M. & Russell, S. J. 436. Coxsackievirus A21 Has Potent Oncolytic Activity in Multiple Myeloma. *Molecular Therapy* **13**, doi:10.1016/j.ymthe.2006.08.502 (2006).

26 Izumchenko, E. *et al.* Patient-derived xenografts effectively capture responses to oncology therapy in a heterogeneous cohort of patients with solid tumors. *Ann Oncol* **28**, 2595-2605, doi:10.1093/annonc/mdx416 (2017).

27 Drapkin, B. J. *et al.* Genomic and Functional Fidelity of Small Cell Lung Cancer Patient-Derived Xenografts. *Cancer Discov* **8**, 600-615, doi:10.1158/2159-8290.CD-17-0935 (2018).

28 Stewart, C. A. *et al.* Single-cell analyses reveal increased intratumoral heterogeneity after the onset of therapy resistance in small-cell lung cancer. *Nat Cancer* **1**, 423-436, doi:10.1038/s43018-019-0020-z (2020).

29 Lemos de Matos, A., Franco, L. S. & McFadden, G. Oncolytic Viruses and the Immune System: The Dynamic Duo. *Mol Ther Methods Clin Dev* **17**, 349-358, doi:10.1016/j.omtm.2020.01.001 (2020).

30 George, J. *et al.* Comprehensive genomic profiles of small cell lung cancer. *Nature* **524**, 47, doi:10.1038/nature14664

https://www.nature.com/articles/nature14664#supplementary-information (2015).

31 Rudin, C. M., Brambilla, E., Faivre-Finn, C. & Sage, J. Small-cell lung cancer. *Nat Rev Dis Primers* **7**, 3, doi:10.1038/s41572-020-00235-0 (2021).

32 Samstein, R. M. *et al.* Tumor mutational load predicts survival after immunotherapy across multiple cancer types. *Nature Genetics*, doi:10.1038/s41588-018-0312-8 (2019).

33 Burroughs, K. D. *et al.* In Vivo Characterization of Seneca Valley Virus (SVV-001), a Novel Oncolytic Picornavirus for Systemic Treatment of Patients with Solid Tumors with Neuroendocrine Features. *CANCER-TARGETED GENE THERAPY: CLINICAL AND PRECLINICAL STUDIES* (2006).

34 Ottonello, S. *et al.* Association Between Response to Nivolumab Treatment and Peripheral Blood Lymphocyte Subsets in Patients With Non-small Cell Lung Cancer. *Front Immunol* **11**, 125, doi:10.3389/fimmu.2020.00125 (2020).

35 Machiels, J. P. *et al.* A phase 1 dose escalation study of the oncolytic adenovirus enadenotucirev, administered intravenously to patients with epithelial solid tumors (EVOLVE). *J Immunother Cancer* **7**, 20, doi:10.1186/s40425-019-0510-7 (2019).

36 Gollamudi, R. *et al.* Intravenous administration of Reolysin, a live replication competent RNA virus is safe in patients with advanced solid tumors. *Invest New Drugs* **28**, 641-649, doi:10.1007/s10637-009-9279-8 (2010).

37 Alnylam Pharmaceuticals, I. ONPATTRO-Prescribing-Information. (2020).

38 Macedo, N., Miller, D. M., Haq, R. & Kaufman, H. L. Clinical landscape of oncolytic virus research in 2020. *J Immunother Cancer* **8**, doi:10.1136/jitc-2020-001486 (2020).

39 Ribas, A. *et al.* Oncolytic Virotherapy Promotes Intratumoral T Cell Infiltration and Improves Anti-PD-1 Immunotherapy. *Cell* **170**, 1109-1119 e1110, doi:10.1016/j.cell.2017.08.027 (2017).

40 Zhu, P. P., Yuan, S. G., Liao, Y., Qin, L. L. & Liao, W. J. High level of intercellular adhesion molecule-1 affects prognosis of patients with hepatocellular carcinoma. *World J Gastroenterol* **21**, 7254-7263, doi:10.3748/wjg.v21.i23.7254 (2015).

41 Staal-van den Brekel, A. J., Thunnissen, F. B., Buurman, W. A. & Wouters, E. F. Expression of E-selectin, intercellular adhesion molecule (ICAM)-1 and vascular cell adhesion molecule (VCAM)-1 in non-small-cell lung carcinoma. *Virchows Arch* **428**, 21-27, doi:10.1007/BF00192923 (1996).

42 Cullis, P. R. & Hope, M. J. Lipid Nanoparticle Systems for Enabling Gene Therapies. *Mol Ther* **25**, 1467-1475, doi:10.1016/j.ymthe.2017.03.013 (2017).

43 Besin, G. *et al.* Accelerated Blood Clearance of Lipid Nanoparticles Entails a Biphasic Humoral Response of B-1 Followed by B-2 Lymphocytes to Distinct Antigenic Moieties. *Immunohorizons* **3**, 282-293, doi:10.4049/immunohorizons.1900029 (2019).

44 Shafren, D. R., Dorahy, D. J., Greive, S. J., Burns, G. F. & Barry, R. D. Mouse cells expressing human intercellular adhesion molecule-1 are susceptible to infection by coxsackievirus A21. *J Virol* **71**, 785-789,

doi:10.1128/JVI.71.1.785-789.1997 (1997).

45 Locy, H. *et al.* Immunomodulation of the Tumor Microenvironment: Turn Foe Into Friend. *Front Immunol* **9**, 2909, doi:10.3389/fimmu.2018.02909 (2018).

46 Haines, B. B. *et al.* ONCR-177, an Oncolytic HSV-1 Designed to Potently Activate Systemic Antitumor Immunity. *Cancer Immunol Res* **9**, 291-308, doi:10.1158/2326-6066.CIR-20-0609 (2021).

47 Khair, D. O. *et al.* Combining Immune Checkpoint Inhibitors: Established and Emerging Targets and Strategies to Improve Outcomes in Melanoma. *Front Immunol* **10**, 453, doi:10.3389/fimmu.2019.00453 (2019).

48 Sivanandam, V., LaRocca, C. J., Chen, N. G., Fong, Y. & Warner, S. G. Oncolytic Viruses and Immune Checkpoint Inhibition: The Best of Both Worlds. *Mol Ther Oncolytics* **13**, 93-106, doi:10.1016/j.omto.2019.04.003 (2019).

49 Hales, L. M. *et al.* Complete genome sequence analysis of Seneca Valley virus-001, a novel oncolytic picornavirus. *J Gen Virol* **89**, 1265-1275, doi:10.1099/vir.0.83570-0 (2008).

50 Newcombe, N. G. *et al.* Enterovirus capsid interactions with decay-accelerating factor mediate lytic cell infection. *J Virol* **78**, 1431-1439, doi:10.1128/jvi.78.3.1431-1439.2004 (2004).

Figures

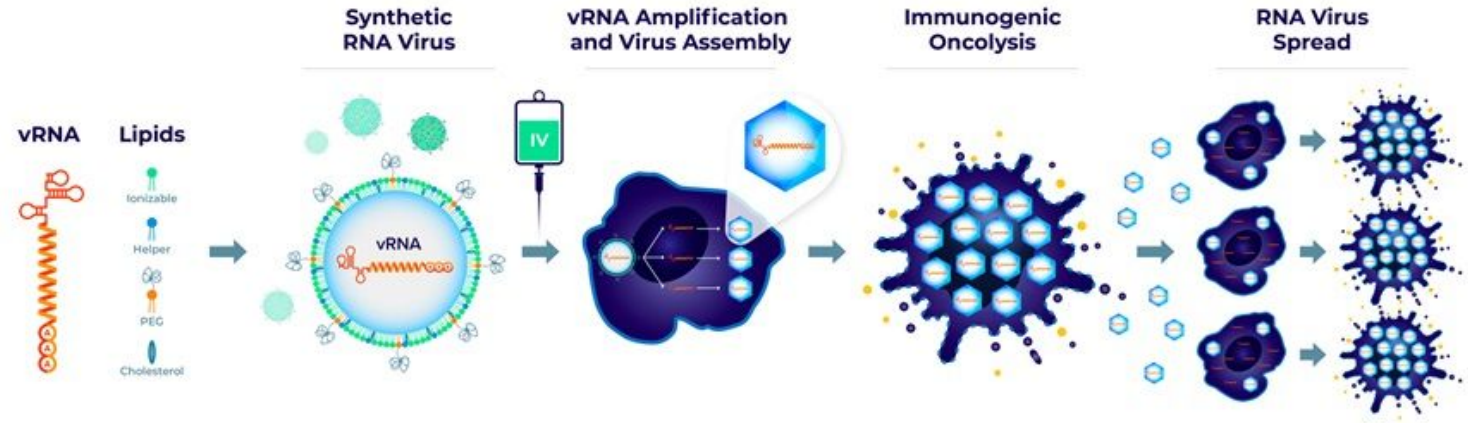

Figure 1

Schematic illustration of the mechanism of action of Synthetic RNA virus. Synthetic RNA virus is comprised of IVT-produced vRNA encapsulated within an LNP. Inside tumor cells, vRNA recapitulates all phases of the viral life cycle such that it replicates and generates a burst of infectious virions that spread locally, infecting, and killing tumor cells, thereby recruiting immune cells to the TME.

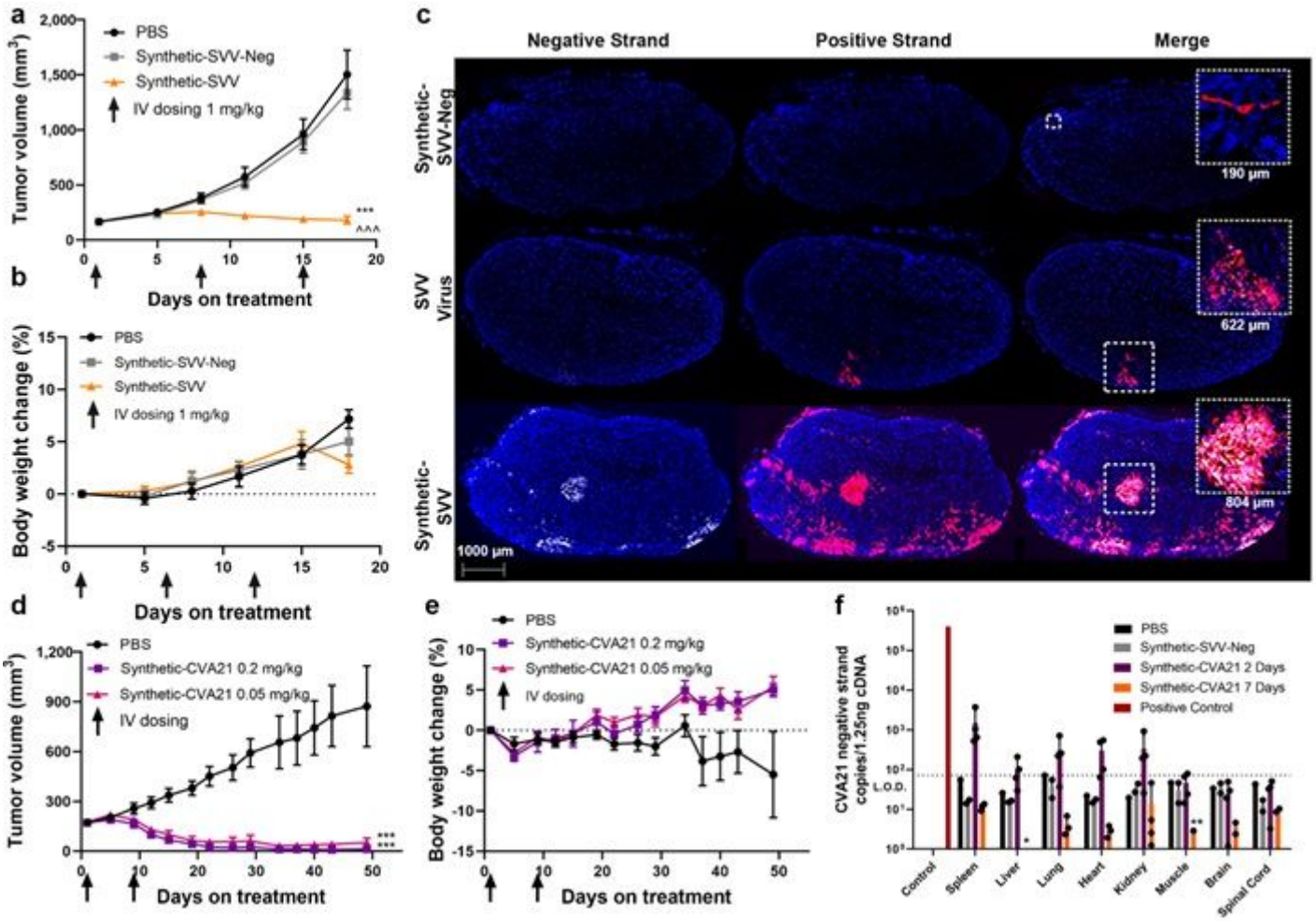

Figure 2

Intravenous Synthetic RNA virus administration demonstrates tumor-specific viral replication and mediates tumor regression. (a-b) Athymic nude mice (n = 8 per group) implanted subcutaneously with NCI-H446 SCLC xenograft tumors were treated via IV administration with either vehicle control (PBS), Synthetic-SVV-Neg, or Synthetic-SVV on Days 1, 8, and 15, at a dose of 1.0 mg/kg. (a) Tumor volume (mm3) and (b) body weight changes (%) were monitored. (c) FISH specific for the SVV positive (red) or the negative (white) strands are shown for a section of whole NCI-H446 xenograft tumors treated with one dose (1 mg/kg) of Synthetic-SVV-Neg, SVV virus, or Synthetic-SVV and collected after 72 hr. The inset is depicted to scale with a white box with inset scales measured directly and included below. (d-e) Athymic nude mice (n = 7 per group) implanted subcutaneously with SK-MEL-28 human melanoma tumors were treated by IV administration with either vehicle control (PBS) or Synthetic-CVA21 on Days 1 and 8 at 2 different doses, 0.2 mg/kg or 0.05 mg/kg. (d) Tumor growth (mm3) and (e) body weight changes (%) were monitored. Statistical significance was determined using a mixed linear model *** $p < 0.001$ vs. PBS and ^^^ $p < 0.001$ vs. Synthetic-SVV-Neg. (f) Viral replication in tissues in huICAM1 transgenic mice (n = 4 per group) after IV administration of Synthetic-CVA21. Tissues (n = 4) were collected after 2- and 7-days post-dosing and RT-qPCR of the CVA21 negative-strand was conducted from tissue homogenates. * and ** indicate samples had replicates with no detectable signal. The positive

control sample is derived from CVA21 infected NCI-H1299 cells in culture. The RT-qPCR limit of detection (LoD) is denoted with a dotted line. Data are reported as mean ± s.e.m.

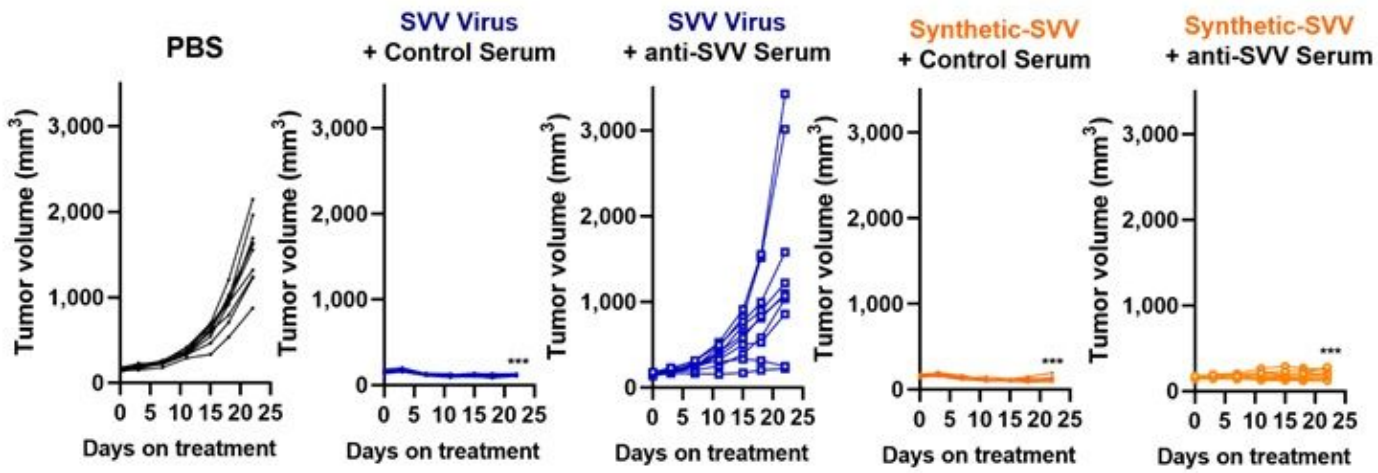

Figure 3

Synthetic-SVV is efficacious in the presence of circulating SVV neutralizing antibodies. Anti-tumor efficacy of SVV virions and Synthetic-SVV as assessed by tumor volume (mm3) was evaluated in NCI-H446 tumor bearing mice after injection of control or anti-SVV rabbit serum. Mice passively immunized to SVV received 2 IV injections of either 106 PFU of SVV virions or 1.0 mg/kg Synthetic-SVV (n = 10 per group). Statistical significance was determined using a mixed linear model *** $p < 0.001$ vs. PBS.

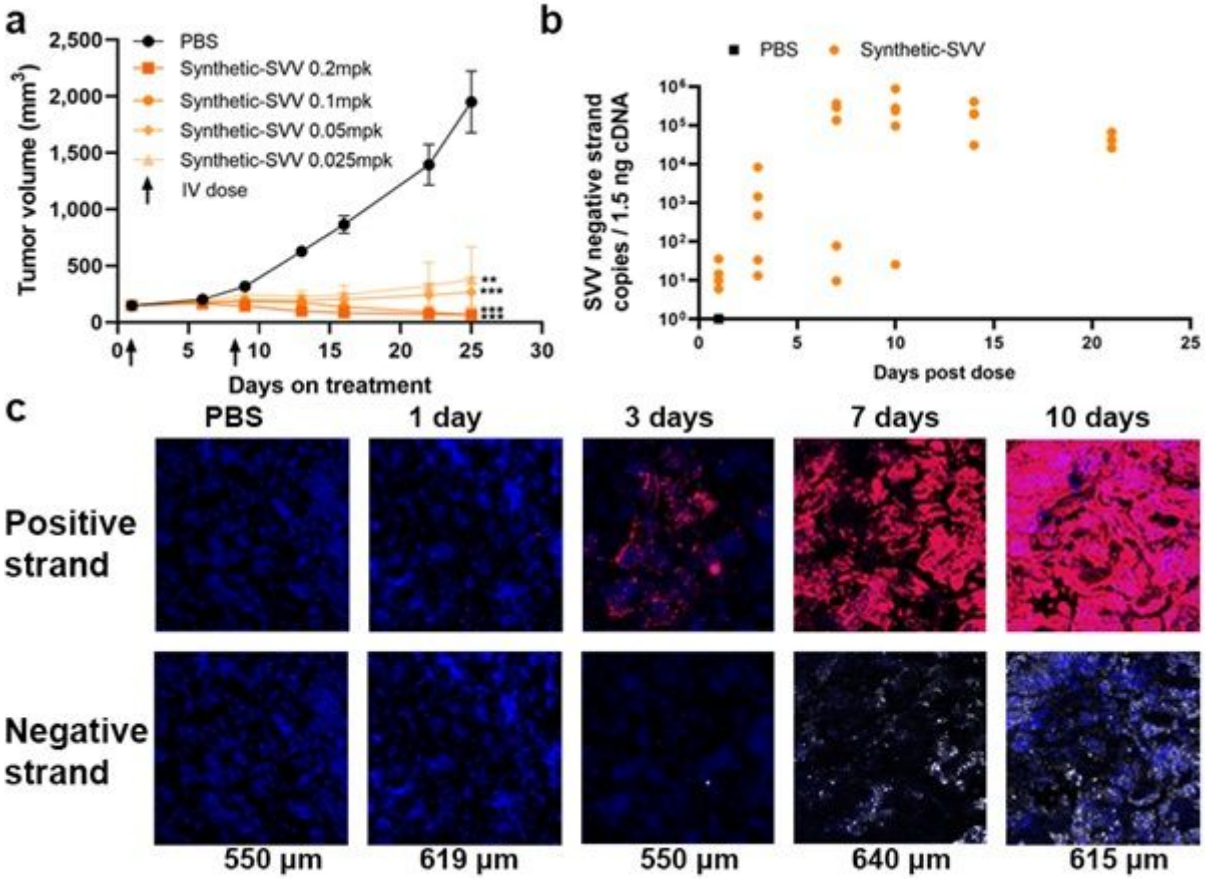

Figure 4

Anti-tumor activity of Synthetic-SVV is dose-dependent and driven by the rapid initiation of SVV replication after systemic administration. (a) Athymic nude mice (n = 7 per group) implanted subcutaneously with NCI-H446 tumors were treated by IV administration with either PBS vehicle control or Synthetic-SVV on Days 1 and 8 at doses ranging from 0.025 to 0.2 mg/kg. (a) Tumor volume (mm3) was monitored. Data are reported as mean ± s.e.m. Statistical significance was determined using a mixed linear model ** p = 0.001 and *** p < 0.001 vs. PBS. (b-c) Replication of Synthetic-SVV in NCI-H446 tumors after a single IV dose of 0.1 mg/kg SVV. (b) SVV negative-strand RNA levels were determined using RT-qPCR (n = 5 per time point). (c) FISH specific for SVV positive and negative strands are shown for NCI-H466 tumor sections.

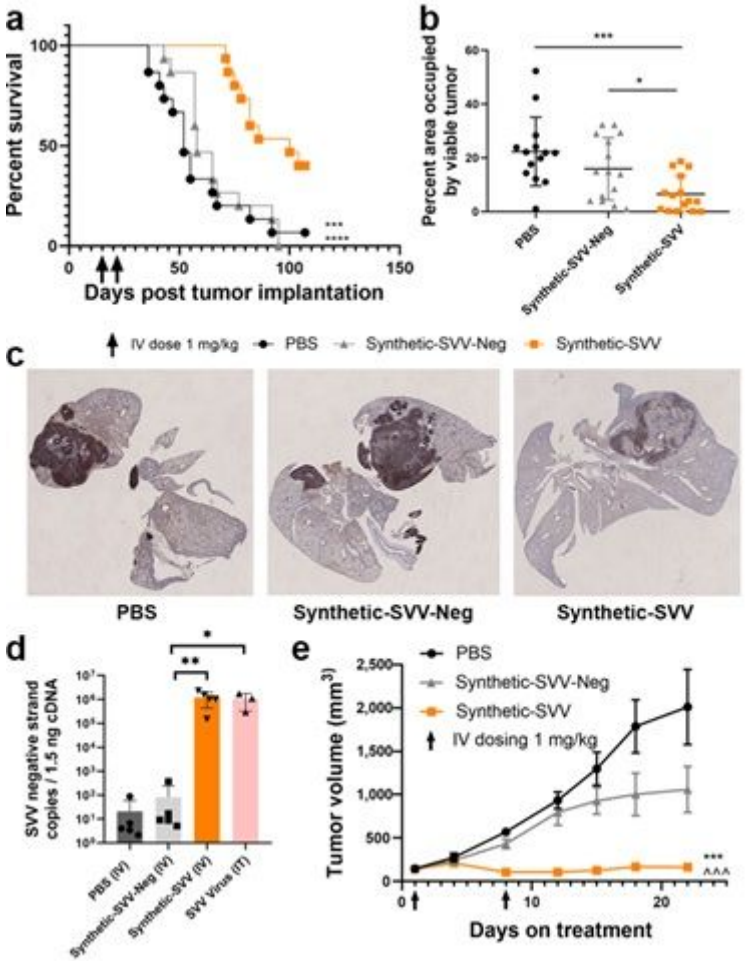

Figure 5

Synthetic-SVV treatment is efficacious and prolongs survival in an orthotopic SCLC model. (a-c) NCI-H82 tumors were orthotopically implanted in athymic nude mice. Animals were dosed either with PBS, 1.0 mg/kg Synthetic-SVV-Neg, or 1.0 mg/kg Synthetic-SVV on Days 15 and 22 post tumor inoculation (n = 15 per group). (a) Survival analysis was assessed using log-rank (Mantel-Cox) test, *** p = 0.0003; **** p < 0.0001 vs. Synthetic-SVV. (b) Morphometric analysis of hDLL3 positive area of pulmonary and extrapulmonary tissue occupied by viable tumor in lungs collected from mice 10 days post-treatment. (c) Representative images of hDLL3 staining. Statistical significance was determined using unpaired T-test * p = 0.011; *** p = 0.003. (d-e) NOD/SCID mice were implanted subcutaneously with SCLC PDX tumors (Crown Bioscience, San Diego, CA) and treated as indicated. (d) Mice were dosed once by IV administration with either vehicle control (PBS), Synthetic-SVV-Neg, or Synthetic-SVV 1 mg/kg or intratumorally twice on Days 1 and 4 with 10e6 PFU SVV virions. Tumor tissues were collected on Day 5 to determine viral replication. SVV negative-strand RNA levels were determined via RT-qPCR (n = 5 per group). Statistical significance was determined using unpaired T-test * p = 0.014; ** p = 0.0084. (e) Mice were dosed by IV administration with either vehicle control (PBS), Synthetic-SVV-Neg, or Synthetic-SVV 1 mg/kg on Days 1 and 8 (n = 8 per group). Tumor volume (mm3) was monitored at various time points. Data are reported as mean ± s.e.m. Statistical significance was determined using mixed linear model, *** p < 0.001 vs. PBS, and ^^^ p < 0.001 vs. Synthetic-SVV-Neg.

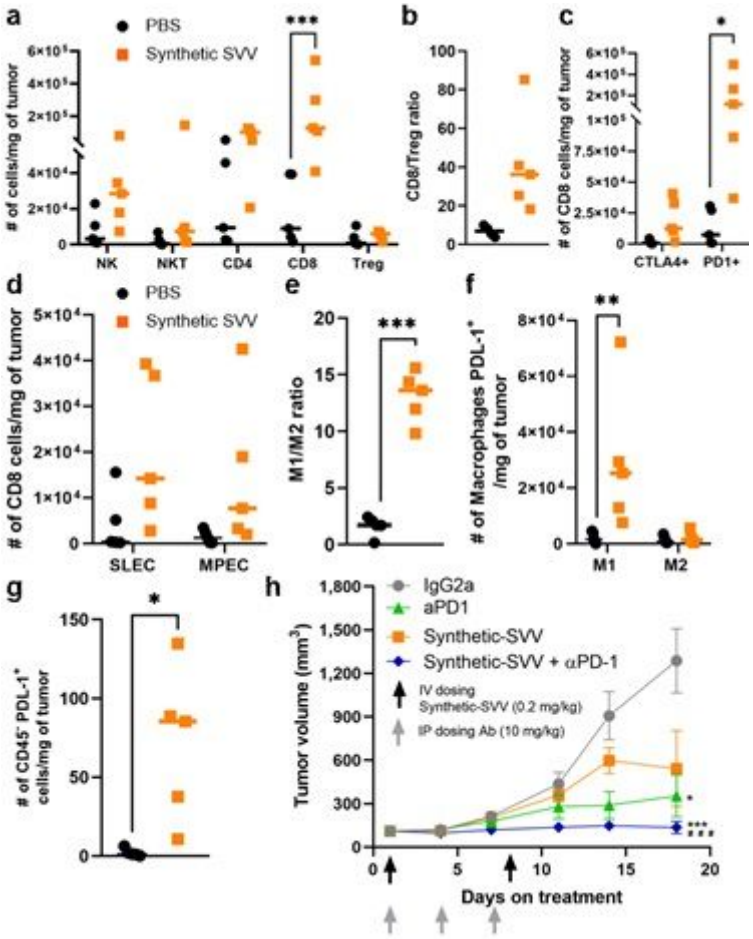

Figure 6

Synthetic-SVV promotes immune cell recruitment and enhances the activity of PD-1 inhibitor. (a-g) A/J mice (n = 5 per group) implanted subcutaneously with syngeneic neuroendocrine N1E-115 tumors. Mice were treated by IV administration with either PBS vehicle control or 1 mg/kg Synthetic-SVV on Days 1 and 8. Tumors were collected 6 days after the second dose. (a) Number of NK, NKT, CD4, CD8, and Treg cells per mg of tumor. (b) CD8/Treg ratio. (c) Number of CD8 T cells per mg of tumor that express CTLA-4 or PD-1. (d) Number of CD8 T cells per mg of tumor that are SLEC (CD127-KLRG1+) or MPEC (CD127+-KLRG1-). (e) Ratio of M1/M2 macrophages. (f) Number of M1 and M2 macrophages PD-L1+ per mg of tumor. (g) Number of CD45- PD-L1+ cells per mg of tumor. (h) A/J mice (n = 10 per group) were implanted subcutaneously with N1E-115 tumors and treated by IV administration with either Synthetic-SVV on Day 1 and 8 (0.2 mg/kg), and IP administration control antibody (mouse IgG2a) or anti-PD-1 antibody on Days 1, 4, and 7 (200 µg) as indicated. Tumor volume (mm3) was monitored. Data are reported as mean ± s.e.m. Statistical significance was determined using a two-way ANOVA test (a, c, d, h), two-tailed paired T-test, * $p < 0.05$, ** $p < 0.01$, *** $p < 0.001$ (b, e, f, g) and a mixed linear model, * $p = 0.03$, *** $p < 0.001$ vs. IgG2a and ### $p<0.001$ vs. Synthetic-SVV.

Supplementary Files

This is a list of supplementary files associated with this preprint. Click to download.

- EditorialChecklist.pdf
- ReportingSummary.pdf
- SupplementalFigures.pdf